Boundary Layer and Cloud Layer Observations Across a Network of 5 Doppler Lidars

Neil P. Lareau, *Department of Meteorology and Climate Science, San José State University, email:neil.lareau@sjsu.edu*

1. Introduction

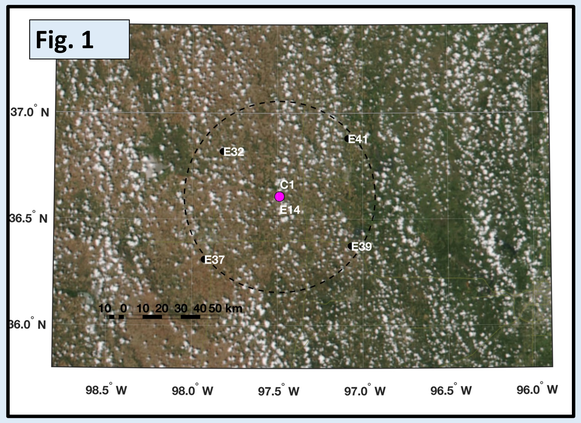

Spatial heterogeneity in the convective boundary layer (CBL) can produce "non-classical mesoscale circulation" (Segal and Arritt 1992), affect the distribution of convective clouds, and potentially contribute to the transition to deep convection (Zhang and Klein 2013). Despite these impacts, the spatial heterogeneity of CBL properties is rarely documented in long term observations.

In this study the spatial variability in the cumulus topped CBL surrounding the ARM-SGP central facility is examined using a network of 5 Doppler lidars. The 5 lidars are distributed within a 50 km radius of the SGP "central facility" (C1, Fig. 1). All sites expect "E32" have eddy correlation (ECOR) surface flux measurements. A sample of 37 shallow cumulus (ShCu) days are used along with a set of 13 days where a transition from shallow to deep convection is observed.

Example day: The spatial variability in ShCu cloud fraction is often observed in satellite imagery, such as is apparent on 17 Sept. 2017 (Fig. 1). Fig. 2a-e shows the corresponding Doppler lidar observations including the CBL vertical velocity (blue and red shading), derived CBL height (dashed black line), and cloud base detections (green dots).

Observed differences include heterogeneity in CBL depth (dashed black line), timing and rate of CBL growth/decay, and the intensity and distribution of updrafts and downdrafts. Commensurate variations in cloud layer properties are also observed. For example, each site shows differences in total cloud fraction, cloud vertical extent. The most pronounced differences are between E41 and the other sites, with E41 having lower CBL height and much lower cloud fraction.

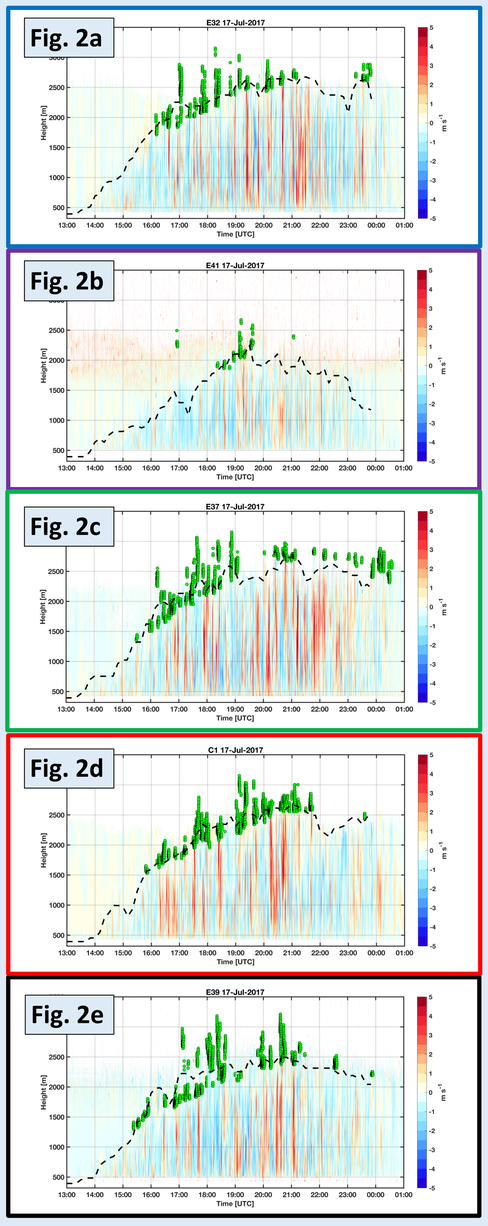

2. Surface Forcing

$$Buoyancy\ Flux = B_0 = \overline{w'b'} = \frac{g}{\rho c_p \overline{T}}\left(\underbrace{SHF + 0.61\frac{c_p\overline{T}}{L_v}LHF}_{Virtual\ Heat\ Flux}\right)$$

$$Sensible\ Heat\ Flux\ (SHF) = \rho c_p \overline{w'T'}$$

$$Latent\ Heat\ Flux\ (LHF) = \rho L_v \overline{w'q_v'}$$

$$Convective\ Velocity\ Scale = w^* = (B_0 Z_i)^{1/3}$$

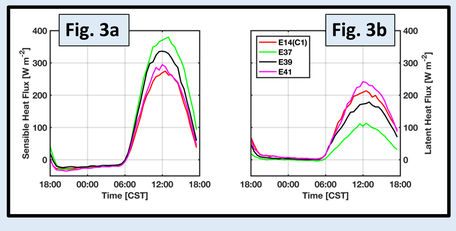

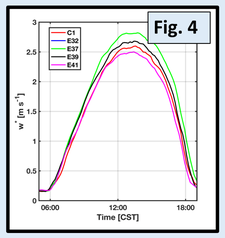

To understand the observed differences in CBL and cloud layer properties it is important to first examine spatial variations in the surface forcing. The surface heat fluxes differ somewhat between sites (Fig. 3). Specifically, E37 has the highest (lowest) sensible (latent) heat fluxes, whereas E41 has the lowest (highest) sensible (latent) heat fluxes. These differences in flux partitioning (i.e., evaporative fraction) are likely related to differences in soil moisture and land use.

The SHF and LHF data are combined to compute a buoyancy flux, and then the convective velocity (w*), which is the forcing for CBL thermals. All sites have similar values of w*, but E37 clearly has the strongest surface forcing for CBL growth and thermal development.

3. Boundary Layer Structure

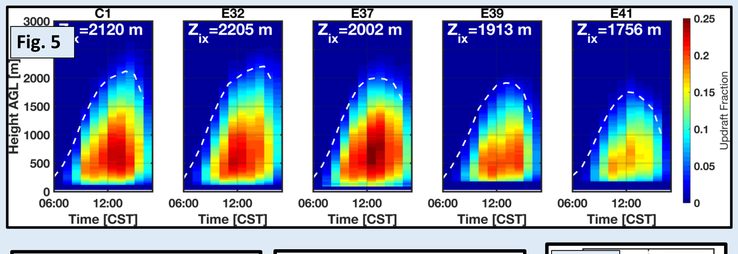

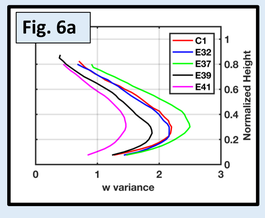

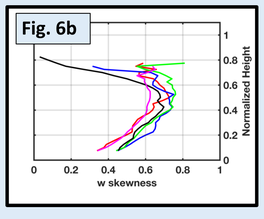

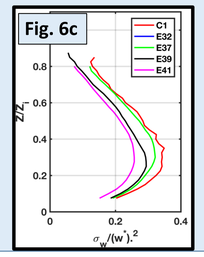

The site-to-site differences in surface forcing produce corresponding differences in CBL depth (dashed white line) and updraft fraction (shading, Fig. 5). The CBL depth is defined by a threshold value in the vertical velocity variance (not shown). The updraft fraction is the fraction of each hour with coherent updraft regions (>1 m s^{-1}, >100 connected pixels). Sites E37 and E41 have the highest and lowest updraft fraction, respectively.

The mid-day (12-14 CST) profiles of vertical velocity variance (Fig. 6a) and skewness (Fig. 6b) also vary across sites. Consistent with the variations in the CBL depth and updraft fraction, E41 has lower skewness and variance than the other sites. The differences in variance remain even after normalizing by the convective velocity, suggesting not all all the site-to-site differences are locally generated (Fig. 6c).

4. Cloud Statistics and Cloud Base Updrafts

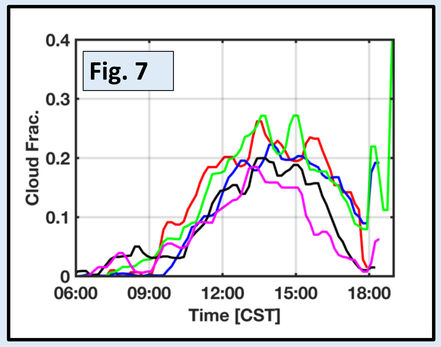

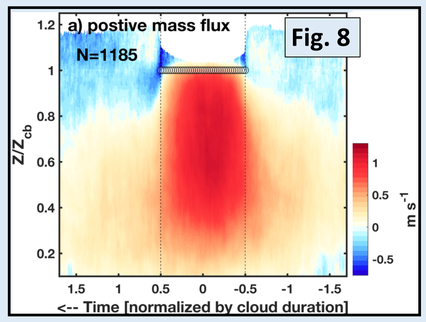

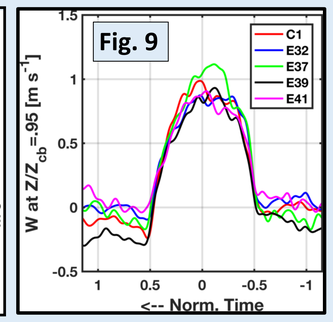

The observed differences in CBL structure also correspond to differences in the cloud fraction (Fig. 7). The maximum cloud fraction (~.27) occurs at C1 and E37, whereas E41 has the lowest cloud fraction. A similar trend is apparent in the case study (Fig. 2). The diurnal cycle is similar across sites, with cloud dissipating earliest at E41.

Figure 8 presents the composite subcloud circulation for all "positive mass flux" clouds across all 5 sites. A coherent subcloud updraft extends through the depth of the CBL and narrow cloud edge downdrafts are observed. When separated by site, modest differences in cloud base updraft (W_{cb}) strength are apparent (Figs. 9, 10). Specifically, stronger updrafts occur more frequently at E37 (Fig 10), the site with the highest convective velocity, updraft fraction, and cloud fraction.

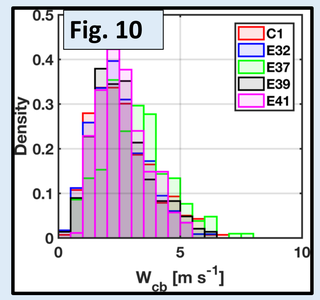

5. Updraft Properties

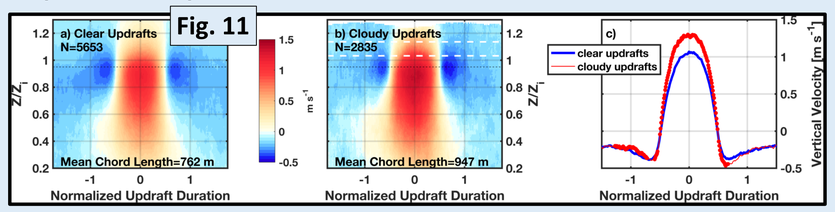

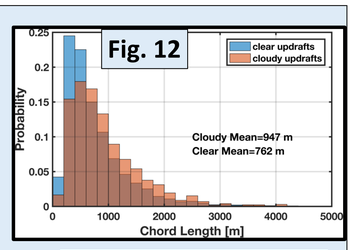

Samples of clear (Fig. 11a) and cloudy (Fig 11b) updrafts in the upper CBL (Z/Zi =.95) are also examined using data from all 5 sites. These two populations have similar updraft/downdraft "triplet" structures, but the cloudy updrafts are systematically stronger (Fig. 11c) and larger (Fig. 12). It is also apparent, from comparing samples (Fig. 11a vs 11b), that both cloudy and cloud free updrafts have distinct mechanically generated downdrafts along their flanks.

The normalized updraft speed (w/w*) in the upper CBL (at Z/Zi=.95) also varies with normalized updraft width (D/Z_i) (Fig. 13), such that wider updrafts are stronger than narrow updrafts. The tendency for cloudy updrafts to be stronger is apparent at all sizes.

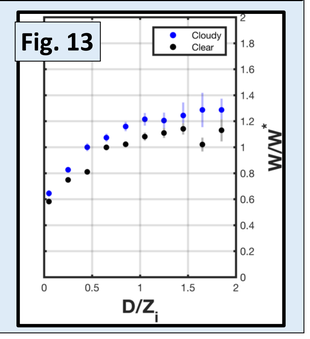

6. Shallow to Deep Convective Transitions

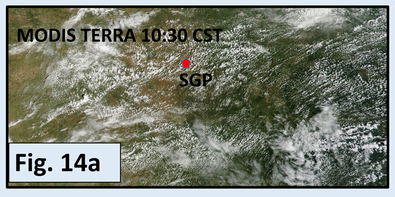

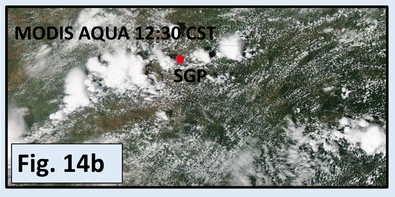

The Doppler lidar network can also be used to examine boundary layer processes during the transition from shallow to deep cumulus convection. Figure 14, for example, shows a day at SGP where local forcing leads to a transition from shallow cumuli in the morning (Fig. 14a) to deep precipitating cumuli in the afternoon (Fig. 14b). The corresponding lidar observations from each of the 5 sites are shown in Figs. 15a-e, revealing a host of CBL and cloud layer processes including cold pools, cloud shading, and penetrative thermals.

Examination of a set of 13 days with locally forced deep convection at SGP show appreciable spatial heterogeneity in the CBL depth amongst the 5 sites (blue line Fig. 16) as compared to the variability observed on days with only ShCu (red line Fig. 16). This difference likely results in part from cold pool processes once convection is initiated, but may also indicate underlying antecedent spatial variability in CBL structure that helps to organize and initiate convection.

Interestingly, there is no clear difference between updraft size and width relationship on days with and without deep convection (Fig. 17) or in the distribution of updraft sizes (not shown). These and other aspects of the CBL structure during transitional days are now the focus of ongoing research

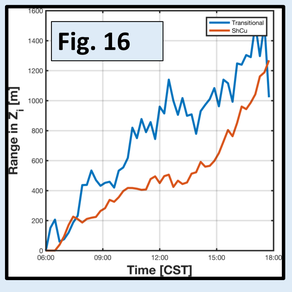

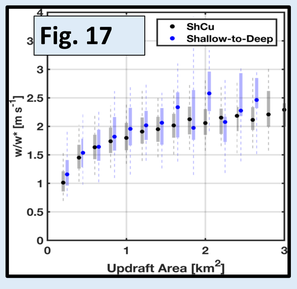

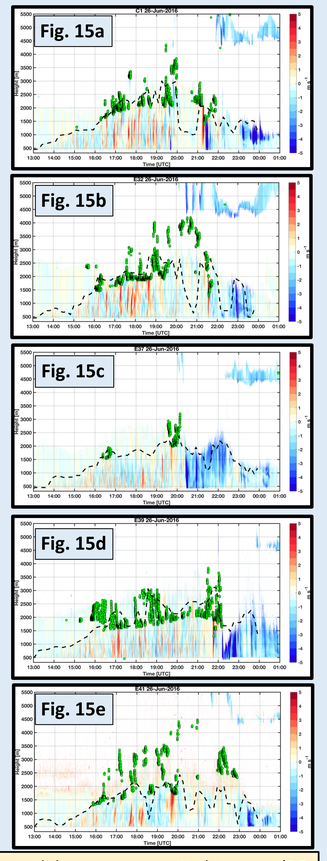

This work is supported by a grant to Neil Lareau (DE-SC0018335) from the Atmospheric Systems Research (ASR) program in the Office of Biological and Environmental Research, Office of Science, Department of Energy